BMC Musculoskeletal Disorders

RESEARCH

Open Access

The neutrophil extracellular trap-related gene FPR1 (formyl peptide receptor 1) as a potential prognostic and therapeutic target in osteosarcoma

Shihao Li[1], Qiong Yuan[2], Yuanyuan Zhang[3] and Haiyang Zhang[3,4*]

Abstract

Background Neutrophil extracellular trap (NET) has been implicated in cancer progression and metastasis. Nevertheless, the role of the NET-related gene, formyl peptide receptor 1 (FPR1), in osteosarcoma (OS) remains largely unexplored. This study aimed to investigate the prognostic significance and biological function of FPR1 in OS.

Methods The least absolute shrinkage and selection operator (LASSO) algorithm was employed to construct a NET-related prognostic model utilizing OS datasets from TARGET and GEO (GSE21257) databases. The scRNA-seq dataset GSE162454 was then used for verifying the role of NET-related model in OS at single-cell resolution. Next, survival analysis and multivariate cox regression analysis were performed to evaluate the prognostic value of FPR1 in OS patients. The CIBERSORT algorithm was conducted to evaluate the relationship between FPR1 levels and immune cell abundance. Subsequently, the biological role of FPR1 was explored through CCK-8, and transwell assays in OS cell lines.

Results A signature NET score, comprising four NET-related genes (TNFRSF10C, FPR1, BST1 and SELPLG), was constructed to predict the prognosis of OS. The survival outcomes for patients in high-NET score group were markedly worse than that in the low-NET score group. Meanwhile, at single cell resolution, OS cells progressively evolved into tumors with elevated NET scores. Furthermore, FPR1 levels were markedly reduced in OS cells when compared to normal osteoblast cells, and the overexpression of FPR1 notably suppressed OS cell viability, migration and invasion. Additionally, OS patients exhibiting high levels of FPR1 demonstrated a favorable overall survival. Moreover, these patients also had a higher proportion of M1 macrophages and a lower proportion of M0 macrophages.

Conclusion Collectively, our study indicates that the NET-related gene FPR1 is closely related to tumor progression, prognosis and immune infiltration in OS.

Keywords Osteosarcoma, Neutrophil extracellular trap, Single cell RNA sequencing, Prognosis, Tumor microenvironment, FPR1

*Correspondence:
Haiyang Zhang
zhangocean666@sina.com

Full list of author information is available at the end of the article

Introduction

Osteosarcoma (OS) is a malignant bone tumor predominantly affecting pediatric and adolescent patients [1]. A large number of studies have indicated that OS displays a high incidence of recurrence and metastasis after therapy [2, 3]. Despite the application of various therapeutic approaches, including surgery and chemotherapy [4], targeted therapy [5], immunotherapy [6] and radio-nanotherapy [7], patients with OS often experience a worse prognosis [8]. Thus, identifying key prognostic indicators is vitally important for predicting outcomes in OS.

Additionally, researchers have confirmed that OS is a bone malignancy characterized by an immunosuppressive tumor microenvironment (TME) [9]. The tumor immune microenvironment (TIME) exerts vital roles in the progression of OS [10]. The immunosuppressive cells residing in the TIME facilitate tumor cells in evading immune detection, eventually leading to the poor prognosis of OS patients [9]. Neutrophils are an important immune cell type in the TME [11], playing important roles in the initiation and metastasis of cancers [12]. Within the TME, certain populations of neutrophils exhibit exert tumor-supportive functions, while other populations have anti-tumoral activities [12–14]. Meanwhile, neutrophil infiltration in some solid cancers, such as glioma and colorectal cancer, has been associated with poor prognosis [15, 16].

Neutrophil extracellular traps (NET) are web-like structures that are constituted by DNA-histone complexes and neutrophil granular proteins [17]. Activated neutrophils can release NET in response to different cues in the TME [17]. The formation of NET may promote tumor growth and metastasis [18–20]. Meanwhile, NET are related to poor prognosis in patients with different cancers, such as glioma and pancreatic cancer [21, 22]. Nevertheless, the function of NET and NET-related genes in OS remains largely unexplored.

Recently, some researchers have established prognostic signatures in cancers based on NET-related genes to predict patient prognosis and tumor immunity [23–25]. For example, Li et al. developed a signature comprising seven NET-related genes, demonstrating its potential to predict the prognosis and immune status of head and neck squamous cell carcinoma patients [26]. In this study, we developed a four NET-related gene signature (TNFRSF10C, FPR1, BST1 and SELPLG) for OS, and found that this signature could reflect the prognosis of OS patients. Additionally, we also investigated the prognostic value of the NET-related gene formyl peptide receptor-1 (FPR1) in OS. FPR1 has been implicated in tumor progression in various cancers [27, 28]. However, the prognostic role of FPR1 in OS remains largely unexplored. Our results showed that FPR1 may serve as an independent predictor for OC prognosis. These findings may provide a foundation for evaluating the prognosis of OS patients in clinical practice.

Materials and methods

Data collection

The clinical and transcriptomic data of 88 OS samples were acquired from the TARGET database (https://ocg.cancer.gov/programs/target). Four samples with incomplete survival (three samples) and clinical (one sample) data were removed, resulting in a final cohort of 84 samples with complete survival information, which was set as the training cohort (TARGET_OS). The data from the TARGET database can be analyzed directly. The characteristics of 84 patients with OS were presented in Table S1.

The GSE21257, GSE162454, GSE16088, GSE19276, GSE99671 and GSE16091 datasets were acquired from the Gene Expression Omnibus (GEO) database (https://www.ncbi.nlm.nih.gov/geo/). GSE21257 dataset included 53 OS samples from 53 patients, comprising 34 patients who developed metastases within 5 years and 19 patients who did not develop metastases within 5 years [29], and this dataset was set as the validation cohort. For this dataset, sequencing was performed using the Illumina human-6 v2.0 expression beadchip (GPL10295) platform to obtain the sequencing data.

GSE16088 comprised 6 normal samples and 14 OS samples, with sequencing processed on Affymetrix Human Genome U133A Array (GPL96) platform. GSE19276 comprised 5 normal samples and 44 OS samples, with sequencing processed on Agilent-012391 Whole Human Genome Oligo Microarray G4112A (GPL6848) platform. GSE99671 dataset comprised 18 OS tissues and 18 non-tumoral paired tissues, with sequencing processed on AB 5500xl-W Genetic Analysis System (GPL20148) platform. GSE16091 dataset comprised 34 OS samples, with sequencing processed on Affymetrix Human Genome U133A Array (GPL96) platform. For all GEO datasets used in this study, an annotation file was utilized to convert probes into gene symbols, which were used for subsequent analysis.

GSE162454 dataset contained single-cell RNA sequencing data from 6 patients with OS [30, 31]. Sequencing for this dataset was conducted using the Illumina NovaSeq 6000 (GPL24676) platform.

Construction of prognostic gene signature

The prognostic model was constructed using the TARGET_OS cohort. A total of 69 NET-related genes [26] were subjected to univariate Cox regression analysis to screen the prognosis-related genes in OS. Next, the least absolute shrinkage and selection operator (LASSO) regression analysis further optimized the prognosis-related genes in OS using the R package (version 4.2.2) "glmnet" [32]. First, the "cv.glmnet" function

was employed to identify the optimal lambda (λ) values. Subsequently, 10-fold cross-validation was conducted, followed by the application of the "coef" function to filter the optimized genes included in the model based on the identified λ values. Meanwhile, these optimized genes were applied for constructing the NET-related signature. The risk score was calculated as follows: risk score (NET score) = $(\text{NET score}) = \sum_{i=1}^{n} Coef_i \times x_i$ [33, 34]. *Coef* represents the coefficient of each optimized gene calculated by the LASSO regression analysis model, and *x* represents the gene expression value of each optimized gene. The value of NET score was determined using the R packages "survival" and "survminer" and a two-sided log-rank test. After that, according to the median NET score, the OS patients were then grouped into high- and low-NET score groups.

Survival analysis

The survival outcomes of OS patients in two groups were assessed using the R packages "survival" and "survminer" (https://CRAN.R-project.org/package=survival) based on Kaplan-Meier method. The log-rank test was applied to evaluate statistical significance of survival outcomes between two groups. Multivariate cox regression analysis was conducted for evaluating whether NET score of FPR1 gene could be an independent predictor of patient survival. The R package "timeROC" was used for drawing receiver operating characteristic (ROC) curves, and the area under the curves (AUC) was then calculated [35].

Gene ontology (GO) analysis, kyoto encyclopedia of genes and genomes (KEGG) enrichment and gene set variation analysis (GSVA) analyses

For screening differentially expressed genes (DEGs) between two NET score groups, R package "edgeR" was used [36]. The criteria for defining DEGs were set as |log2(fold change)| >0.5 and p.adjust < 0.05. The DEGs between two groups were subjected to GO analysis and KEGG enrichment analysis using the R package "clusterProfiler" [37]. GO analysis included biological process (BP), molecular function (MF) and cell composition (CC) analysis. P-value < 0.05 was considered to be significant.

For the GSVA, the "c2.cp.kegg.v2023.1.Hs.symbols" and "c5.go.v2023.1.Hs.symbols" gene sets were acquired from the Molecular Signature Database (https://www.gsea-msigdb.org/gsea/msigdb). The threshold for significanc e was set to a P-value < 0.05.

Single-cell RNA-sequencing (scRNA-seq) analysis

The scRNA-seq data from OS samples, downloaded from GSE162454 dataset, was pre-processed with the R package "Seurat" [38]. After removing low-quality cells (cells that have less than 200 genes expressed and mitochondrial gene expression exceeding 5%), the data was normalized using the function 'NormalizedData'. Next, the principal component analysis (PCA) was conducted with the function "RunPCA". Unsupervised clustering analysis was then conducted to identify the main cell type using the function "FindCluster" in R package "Seurat", and the t-SNE algorithm was used for visualization. After that, the R package 'Single R' was used for the annotation of the cell clusters [39], this package contains 5 human databases and 2 mouse databases, with the "Human Primary Cell Atlas Data (HPCA)" database utilized for annotation. Meanwhile, we performed "FindMarkers" function, setting the logfc.threshold to 0.25 and min.pct to 0.1, to identify DEGs between two NET score groups. Additionally, the R package "monocle" was performed to proceed the pseudotime trajectory analysis to observe the progression of continuous cell states [40]. Furthermore, cell communication pattern was established by the R package "iTALK" (https://github.com/Coolgenome/iTALK).

Gene set enrichment analysis (GSEA)

In the TARGET_OS cohort, OS patients were divided into FPR1-high and FPR1-low groups based on the median expression value of FPR1. For screening DEGs between two groups, R package "DESeq2" was used [41]. The criteria for defining DEGs were set as |log2(fold change)| >1 and p.adjust < 0.05. GSEA was conducted using the R package "clusterProfiler", with a pathway considered significant if p.ajust < 0.05 [42].

Analysis of immune cell characteristics

The CIBERSORT software (version 0.1.0) was employed in this study to determine the relative proportions of 22 types of immune cells in each sample. In each sample, the sum of all estimated immune cell type proportions is equal to 1. The ESTIMATE algorithm (https://R-Forge.R-project.org/projects/estimate/) was utilized to assess the immune score, stromal score and estimate score.

Cell culture and transfection

The HFOB1.19 cell line (GNHu14, National Collection of Authenticated Cell Cultures) was cultured in DMEM medium (No. PM150270, Procell) supplemented with 10% FBS (No. PM164210, Procell) and 1% P/S (No. P1400, Procell), and maintained at 34℃ in a humidified atmosphere with 5% CO_2. The HOS cell line (CL-0360, Procell) was cultured in MEM medium (No. PM150410, Procell) supplemented with 10% FBS and 1% P/S. The U-2OS (CL-0236, Procell) and SAOS-2 (iCell-h313, The World Cell Factory) cell lines were cultured in McCoy's 5 A medium (No. PM150710, Procell) supplemented with 10% FBS and 1% P/S. HOS, U-2OS and SAOS-2 cell lines were maintained at 37℃ in a humidified atmosphere with 5% CO_2.

U-2OS cells were transfected with FPR1 overexpression (OE-FPR1) or negative control (OE-NC) plasmids using a Lipocat2000C transfection reagent (No. AQ11669, Beijing Aoqing Biotechnology Co., Ltd).

Reverse transcription quantitative real-time polymerase chain reaction (RT-qPCR)

Total RNA isolation was performed using the TriQuick Reagent Total RNA Extraction reagent (No. R1100, Solarbio). Next, RNA was reverse transcribed into cDNA using an Evo M-MLV reverse transcription Kit (No. AG11706-S, Accurate Biology) on a PCR instrument (Vapo protect, Eppendorf). Quantitative PCR was conducted using the 2×SuperStar Universal SYBR Master Mix (CW3360, CWBIO) on a quantitative PCR instrument (SLAN-96S, Shanghai Hongshi Medical Technology Co., LTD). The qPCR thermocycling conditions were as follows: predenaturation at 95°C for 30 s, 40 cycles of denaturation at 95°C for 10 s and annealing at 60°C for 30 s. The relative gene expression was calculated by $2^{(-\Delta\Delta CT)}$ method and GAPDH was used as an internal control [43]. FPR1: 5'-GCTCCTCACATTGCCAGTTAT-3' (forward) and 5'- CGTTGGTCCAGGGCGAAAA-3' (reverse); GAPDH: 5'-GAAGGTGAAGGTCGGAGTC-3' (forward) and 5'-GAAGATGGTGATGGGATTTC-3' (reverse).

Western blot assay

Cells were lysed using the RIPA reagent (No. R0010, Solarbio) to obtain total protein. Next, a BCA protein detection kit (No. CW0014S, CWBIO) was conducted to determine protein concentration. Equal amounts of protein samples (30 μg per lane) were separated using 10% SDS-PAGE gels (One-Step PAGE Gel Fast Preparation Kit, No. E303-1, Vazyme) and transferred onto polyvinylidene difluoride membranes (IPVH00010, Merck). The membranes underwent a blocking step using 5% skimmed milk (No. D8340, Solarbio) in TBST (No. T1081, Solarbio) for 1 h, and then incubated with primary antibodies at 4 °C overnight, including anti-FPR1 (1:1000; R1511-36, HUABIO) and anti-GAPDH (1:10000; No. 60004-1-Ig, Proteintech) primary antibodies. After that, the membranes were treated with appropriate secondary antibodies (1:10000; No. ZB-2301, ZB-2305, ZSGB-BIO), an electrochemiluminescence Plus ultrasensitive liquid (No. P0018M, Beyotime) was used for visualization the protein bands. ImageJ software was employed to analyze the gray value of the protein bands and the FPR1 relative expression was quantified as the gray value of FPR1 by the gray value of GAPDH.

Cell counting kit-8 (CCK-8) assay

Cells (5000 cells per well) were plated onto a 96-well plate and allowed to culture overnight. Subsequently, 100 μl of CCK-8 solution (No. C0037, Beyotime) was added to each well, and the plate was then incubated at 37 °C for 3 h. The optical density (OD) values of each well were obtained at a wavelength of 450 nm using a microplate reader (Infinite F50, TECAN).

Transwell assay

Cells (5×10^4 cells) were suspended in 100 μl of medium containing 0.1% FBS and seeded into the upper chamber of inserts in a 24-well plate (No. TCD010100, BIOFIL), and 600 μL of medium containing 10% FBS was loaded to the lower chamber. Following incubation for 24 h, the cells were stained with 0.1% crystal violet (No. Q/12GF, Tianjin Guangfu Fine Chemical Research Institute) for 1 h. After staining, the bottom surface of the Transwell membrane was allowed to air-dry, and images were captured using a light microscope (IMT-2, OLYMPUS). For invasion analysis, Matrigel matrix (356234, BD) was precoated onto the upper chamber of the Transwell.

Statistical analysis

The Wilcoxon rank-sum test was used for comparing values between two groups. Pearson correlation analysis was performed using the function "cor" in R package. Statistical analysis of bioinformatics data was performed using the R software (version 4.2.2). For the experimental results, data were statistically analyzed using GraphPad Prism 9.5.0 software, and one-way ANOVA or two-way ANOVA was used for analyzing the differences among multiple groups; all data are presented as means ± standard deviations (SD). P-values < 0.05 were considered significant.

Results

Construction of NET-related signature in OS

To establish a NET-related signature for OS, 69 NET-related genes (Table S2) were applied in the univariate Cox regression analysis within a TARGET_OS cohort ($n = 84$) [26]. 17 NET-related genes demonstrated prognostic potential in OS (Fig. 1A). Thereafter, LASSO analysis was conducted to further screen the remaining 17 genes, ultimately identifying 4 optimal prognostic NET-associated genes, including tumor necrosis factor receptor superfamily, member 10c (*TNFRSF10C*), *FPR1*, bone marrow stromal cell antigen-1 (*BST1*) and Selectin P ligand gene (*SELPLG*) (Fig. 1B). The LASSO cox model included 4 genes and the prognostic NET-related signature was developed using a linear combination of the expression levels of these 4 genes (Expr) weighted by their LASSO regression coefficients. The formula was as follows: NET score = (-0.10971154 * Expr *TNFRSF10C*) + (-0.04142253 * Expr *FPR1*) + (-0.07035219 * Expr *BST1*) + (-0.01959448 * Expr *SELPLG*). Finally, a four-gene NET-related signature comprising TNFRSF10C, FPR1, BST1, and SELPLG was constructed.

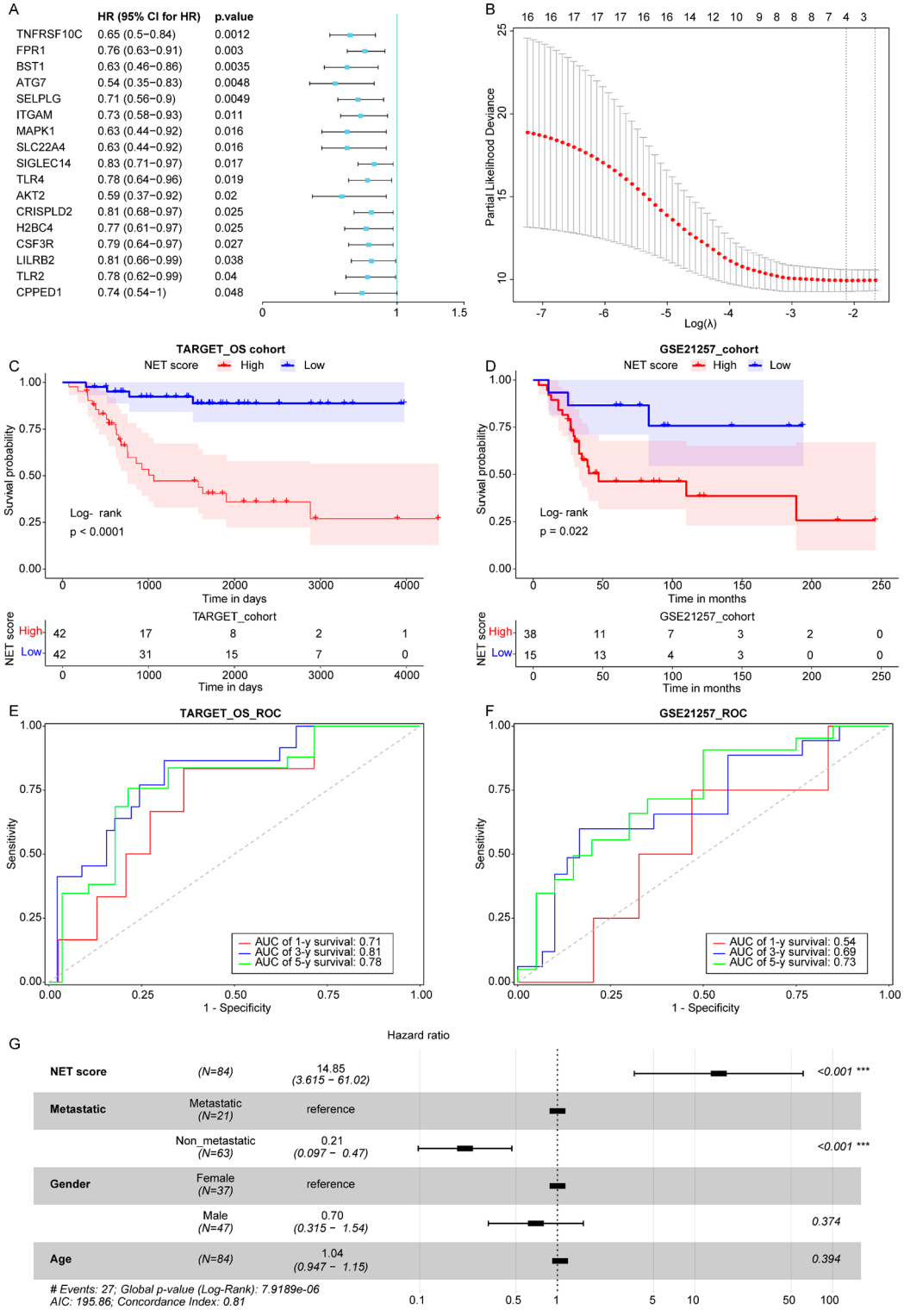

Fig. 1 Construction of NET-related signature in OS. (**A**) A forest map showed 17 NET-related genes identified by univariate Cox regression analysis in the TARGET_OS cohort (**B**) Identification of 17 prognostic NET-related genes using the LASSO regression analysis. The left vertical dotted line indicates the lambda (λ) value with the minimum error and the largest λ value. Under this condition, the constructed model demonstrates the best fitting performance. Therefore, 4 optimal prognostic NET-associated genes, including TNFRSF10C, FPR1, BST1 and SELPLG were identified (**C, D**) Kaplan-Meier survival curves of overall survival in the (**C**) TARGET_OS cohort and (**D**) GSE21257 cohort based on NET score (**E, F**) Time-dependent ROC curves assessing the accuracy of NET score in predicting survival of OS patients at 1-year, 3-year, 5-year in the (**E**) TARGET_OS cohort and the (**F**) GSE21257 cohort (**G**) The multivariate Cox regression analyses of the NET score in the TARGET_OS cohort

Meanwhile, based on the median value of NET score, OS patients were separated into two NET score groups (low-NET and high-NET) in the TARGET_OS cohort. Survival analysis showed that the OS patients with high-NET scores experienced poorer survival outcomes compared to those with low-NET scores (Fig. 1C). Subsequently, OS patients in a validation GSE21257 cohort were separated into two NET score groups based on the optimum cutoff value of the NET score. Similarly, in the validation set, OS patients in the high-NET group displayed shortened survival outcomes compared to the low-NET group (Fig. 1D). Additionally, ROC analysis revealed that the AUC values of 1-, 3-, and 5-year curves were 0.71, 0.81, and 0.78 in the TARGET_OS cohort (Fig. 1E) and were 0.54, 0.69, and 0.73 in the GSE21257 cohort, respectively (Fig. 1F). Furthermore, based on the data in the TARGET_OS cohort, the results of multivariate cox regression analysis showed that NET score may serve as an independent predictor of survival for OS patients (Fig. 1G).

Prognostic value of NET score in OS

To further evaluate the prognostic value of the NET score, we analyzed the association between the NET score and the clinical features of OS patients, including age, sex and metastasis status in the TARGET_OS cohort. OS patients under 18 years of age with high-NET scores exhibited strongly worse survival outcomes compared to those with low-NET scores (Fig. S1A). Meanwhile, OS patients in the female, male and non-metastatic subgroups with high-NET scores showed significantly worse survival outcomes compared to the patients with low-NET scores (Fig. S1B-S1D). Nevertheless, no obvious differences in NET scores were observed between groups with different ages (age ≥ 18 and < 18), genders (female and male) or metastasis status (metastatic and non-metastatic) in the TARGET_OS cohort (Fig. S1E-S1G). Significantly, the NET score was found to be upregulated in metastatic OS samples compared to non-metastatic samples in the GSE21257 cohort (Fig. S2). Collectively, the prognosis of OS patients may be predicted using the established NET-related prognostic signature model.

DEGs and the distinct functional pathways

To investigate the underlying mechanism of the NET-related signature in OS, DEGs between two NET score groups were screened. Significantly, a total of 640 DEGs were detected between high-NET and low-NET groups in the TARGET_OS cohort (Table S3). Compared with the low-NET group, 225 upregulated DEGs and 415 downregulated DEGs, were identified in the high-NET group (Figure S3A, S3B and Table S3). GO and KEGG analysis was then performed on upregulated and downregulated DEGs, respectively. The results revealed that the 225 upregulated DEGs were notably enriched in 84 GO terms and 7 KEGG pathways, and the 415 downregulated DEGs were enriched in 624 GO terms and 39 KEGG pathways (Figure S3C, S3D and Table S4). Thereafter, GSVA results showed that 9 signaling pathways, such as cellular response to macrophage colony stimulating factor stimulus, positive regulation of T cell tolerance induction and positive regulation of lymphocyte anergy, were related to the NET score in OS (Figure S3E).

scRNA-seq analysis for NET score

Based on the data from GSE162454 dataset, scRNA-Seq analysis was used for verifying the role of NET score in OS at single cell resolution. The "FindCluster" function in R package "Seurat" was used to cluster the cells, resulting in the identification of 8 major cell clusters (Fig. 2A). According to the formula (NET score) mentioned above, the NET score for each cell within 8 cell clusters was calculated, with the NET score levels in these clusters presented in Fig. 2B. Subsequently, all cells were categorized into high-NET and low-NET groups based on the median value of the NET score, resulting in the identification of 782 differentially expressed hypervariable genes between the two NET score groups (Table S5). Following this, the biological roles of these 782 genes were identified using the GO and KEGG enrichment analysis. The results revealed that these genes were significantly enriched in 1708 GO terms (e.g. positive regulation of cell activation) and 94 KEGG pathways (e.g. Cytokine-cytokine receptor interaction, antigen processing and presentation and Natural killer cell mediated cytotoxicity) (Fig. 2C and D and Table S6).

Pseudotime analysis identified 3 differentiation stages of OS cells (Fig. 2E). As the pseudotime elevated (Fig. 2F), OS cells showed a tendency toward elevated NET scores (Fig. 2G).

Cell communication pattern

Cell communication between OS cells and other cells in TME was analyzed between two NET score groups with R package "iTALK". The different cellular signaling pathways (CSPs) regarding checkpoints among different cells in the TME were shown in Fig. 3A and B. CD24 was the most active CSPs in OS cells from patients with high-NET scores (Fig. 3A and B). The different CSPs regarding cytokine among different cells in the TME were shown in Fig. 3C and D. CXCL12 and IL1R1 were identified as the most active CSPs in OS cells from patients with high-NET scores (Fig. 3C and D). The different CSPs regarding growth factors among different cells in the TME were shown in Fig. 3E and F, with ITGB1, TGFB1 and CTGF being the most active CSPs in OS cells from patients with low-NET scores (Fig. 3E and F). The different CSPs regarding other aspects among different cells in the TME

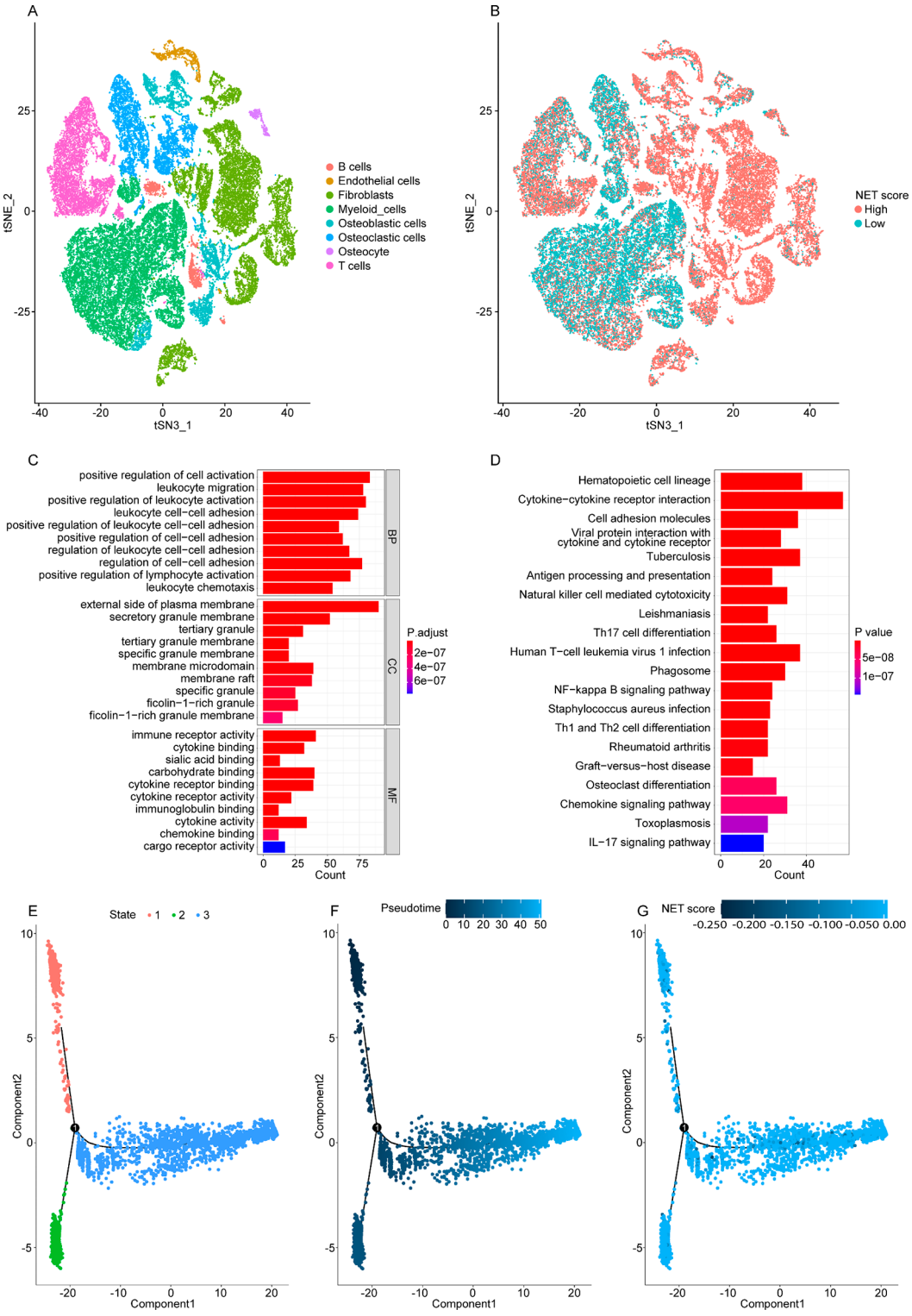

Fig. 2 scRNA-seq analysis for NET score (**A**) The tSNE algorithm was used for visualization of the separate cell clusters in the tumor microenvironment of OS (**B**) The tSNE visualization of cell clusters with high- or low-NET score (**C, D**) The biological roles of 782 differentially expressed hypervariable genes were identified using the GO and KEGG analysis. (**C**) Top 10 enriched GO terms of BP, CC, and MF. (**D**) Top 20 enriched KEGG pathways (**E**) The pseudotime trajectory analysis of OS cells from different differentiation stages. The horizontal and vertical axes represent the two principal components. Each point represents an individual cell. Different colors represent different cell stages. The black circle indicates the branch nodes, where cells can progress toward one of several outcomes. The pseudotime trajectory analysis showed that OS cells can develop into three different cell states (**F**) The pseudotime trajectory analysis of pseudotime pattern on OS cells. The colors from dark to light represent the forward order of pseudotime (**G**) The pseudotime trajectory analysis of NET score on OS cells. The lighter the color, the higher the NET score

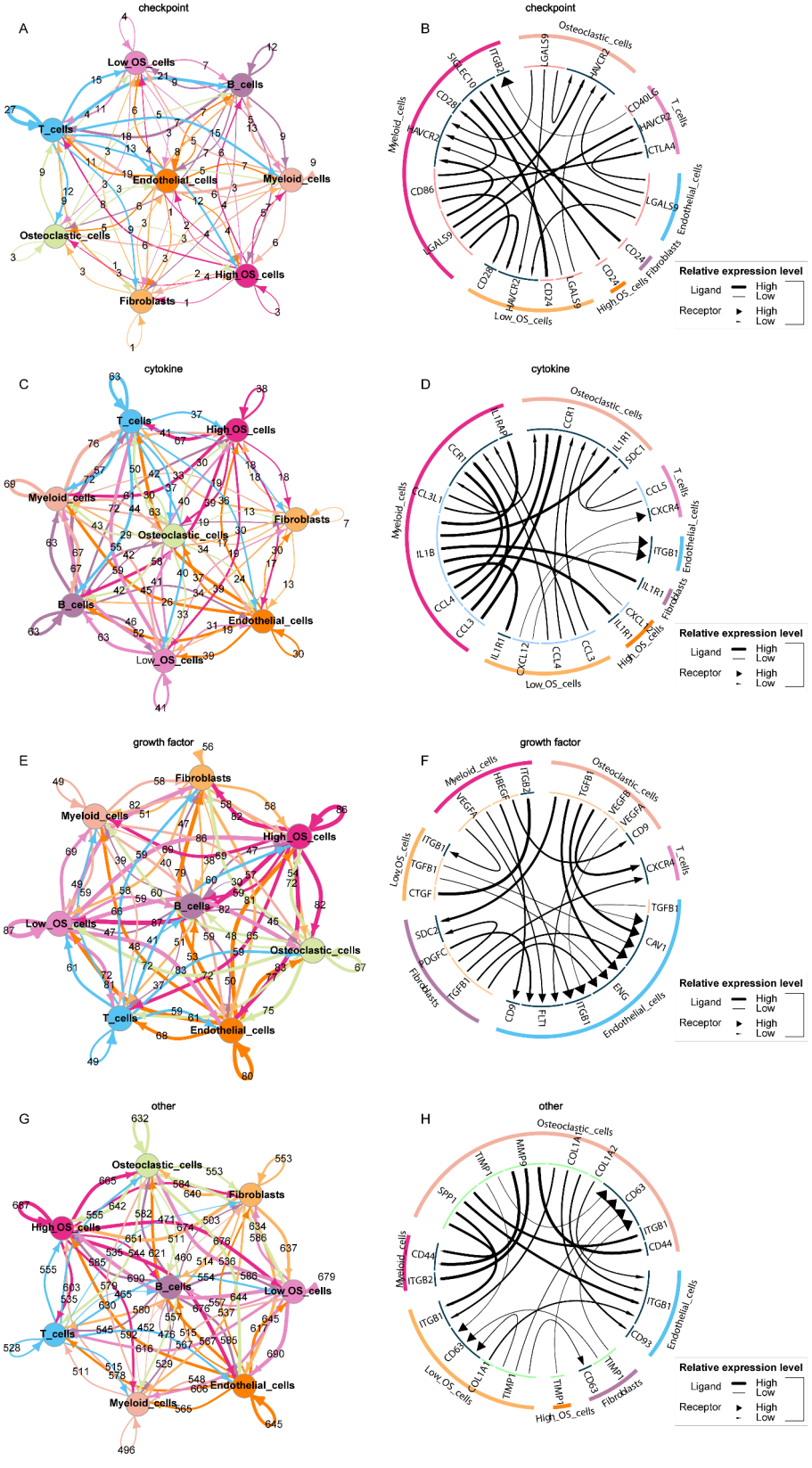

Fig. 3 (See legend on next page.)

(See figure on previous page.)

Fig. 3 Cell communication pattern of high- and low-NET score OS groups (**A, C, E, G**) Different cellular signaling pathways and (**B, D, F, H**) cell communication patterns regarding (**A, B**) checkpoint, (**C, D**) cytokine, (**E, F**) growth factor or (**G, H**) other between two NET score groups of OS cells and other cells in the microenvironment. (**A, C, E, G**) The various colors of the filled circles represent distinct cell types. The circle that emits the arrow represents the ligand cell subpopulation, and the circle that receives the arrow represents the receptor cell subpopulation. The number on the line indicates the number of ligand-receptor interaction pairs. (**B, D, F, H**) The arrows indicate the directionality of the signal (ligand to receptor)

were shown in Fig. 3G and H. TIMP1 was recognized as the most active CSPs in OS cells from patients with high-NET scores (Fig. 3G and H).

Predictive value of NET score in anti-tumor agents

The prediction of drug sensitivity was conducted using the R package "oncoPredict" in the TARGET_OS cohort. The correlation between the NET score and the IC50 value of anti-tumor drugs was analyzed. NET score exhibited a significant negative correlation with two drugs, including SB505124_1194 (a selective TGFβR inhibitor) and BI.2536_1086 (PLK inhibitor) (Fig. 4A and B and Table S7). Next, Comparative Toxicogenomics Database (CTD) database (http://ctdbase.org/) was used to analyze the inference score of NET-associated genes in the NET score in OS. Our findings suggested that TNFRSF10C (Fig. 4C), FPR1 (Fig. 4D), BST1 (Fig. 4E) and SELPLG (Fig. 4F) may serve as the potential therapeutic targets for OS. The strong value of TNFRSF10C and FPR1 in OS development was predicted based on their inference score (Fig. 4C and D).

Prognostic value of FPR1 in OS

Next, we continue to explore the role of FPR1 in the prognosis of OS. Based on the data in the GSE16088, GSE19276 and GSE99671 datasets, the expression level of FPR1 was notably reduced in OS tissues compared to normal controls (Fig. 5A - 5C). Additionally, based on the median expression level of FPR1, OS patients were categorized into two groups (low-FPR1 and high-FPR1) in the TARGET_OS and GSE21257 cohorts, respectively. The results of survival analysis showed that the OS patients in the low-FPR1 group exhibited poorer survival outcomes compared to those in the high-FPR1 group (Fig. 5D and E). Moreover, the results of multivariate cox regression analysis showed that FPR1 may serve as an independent predictor of survival for OS patients (Fig. 5F).

Furthermore, the results of GSEA showed that high-FPR1 group had significant enrichment in 83 pathways, such as Antigen processing and presentation, Apoptosis, Natural killer cell mediated cytotoxicity and Necroptosis, compared to the low-FPR1 group (Fig. 6A and D and Table S8).

Predictive value of FPR1 in immune microenvironment of OS

Next, CIBERSORT software was used to explore the relationship between FPR1 and TIME in OS patients. As shown in Fig. 7A and B, significant differences were observed in M0 macrophages, M1 macrophages, M2 macrophages, Neutrophils, CD4 naïve T cells and Regulatory T cells (Tregs) between high-FPR1 and low-FPR1 groups. Additionally, patients in the high-FPR1 group exhibited elevated stromal, immune and ESTIMATE scores compared to those in the low-FPR1 group (Fig. 7C - 7E). Collectively, FPR1 may be associated with the immune infiltration in OS.

Overexpression of FPR1 suppressed the viability, migration and invasion of OS cells

RT-qPCR was conducted to validate the expression levels of FPR1 in OS cell lines. As indicated in Fig. 8A, FPR1 levels were notably decreased in HOS, SAOS-2 and U2OS cells compared to HFOB1.19 cells. Notably, U2OS cells exhibited the lowest expression level of FPR1, which was utilized in the subsequent experiments (Fig. 8A). As shown in Fig. 8B and C, the expression of FPR1 was notably upregulated in U2OS cells transfected with OE-FPR1 plasmids. Additionally, the results of CCK-8 and transwell assays showed that overexpression of FPR1 remarkably suppressed the viability, migration and invasion of U2OS cells (Fig. 8D and E). These results showed that FPR1 may play a tumor-suppressive role in OS.

Discussion

The formation of NET is a part of the innate immune system [44]. NET can be generated within the TME, which is linked to tumor occurrence and metastasis [45, 46]. Evidence suggested that NET formation facilitates tumor progression and metastasis [45, 47]. Moreover, some researchers have identified a prognostic signature for human cancers based on NET and found that NET-related signature can predict the prognosis of various cancers, such as breast, bladder, lung cancers and OS [23, 25, 48, 49]. However, the potential prognostic values of NET-related signature in OS have not been fully explored.

In the TARGET_OS cohort, we identified 4 prognostic NET-associated genes TNFRSF10C, FPR1, BST1 and SELPLG using the LASSO regression analysis. All these four genes have been implicated in the prognosis of cancer patients [50–54]. Our findings indicated that OS

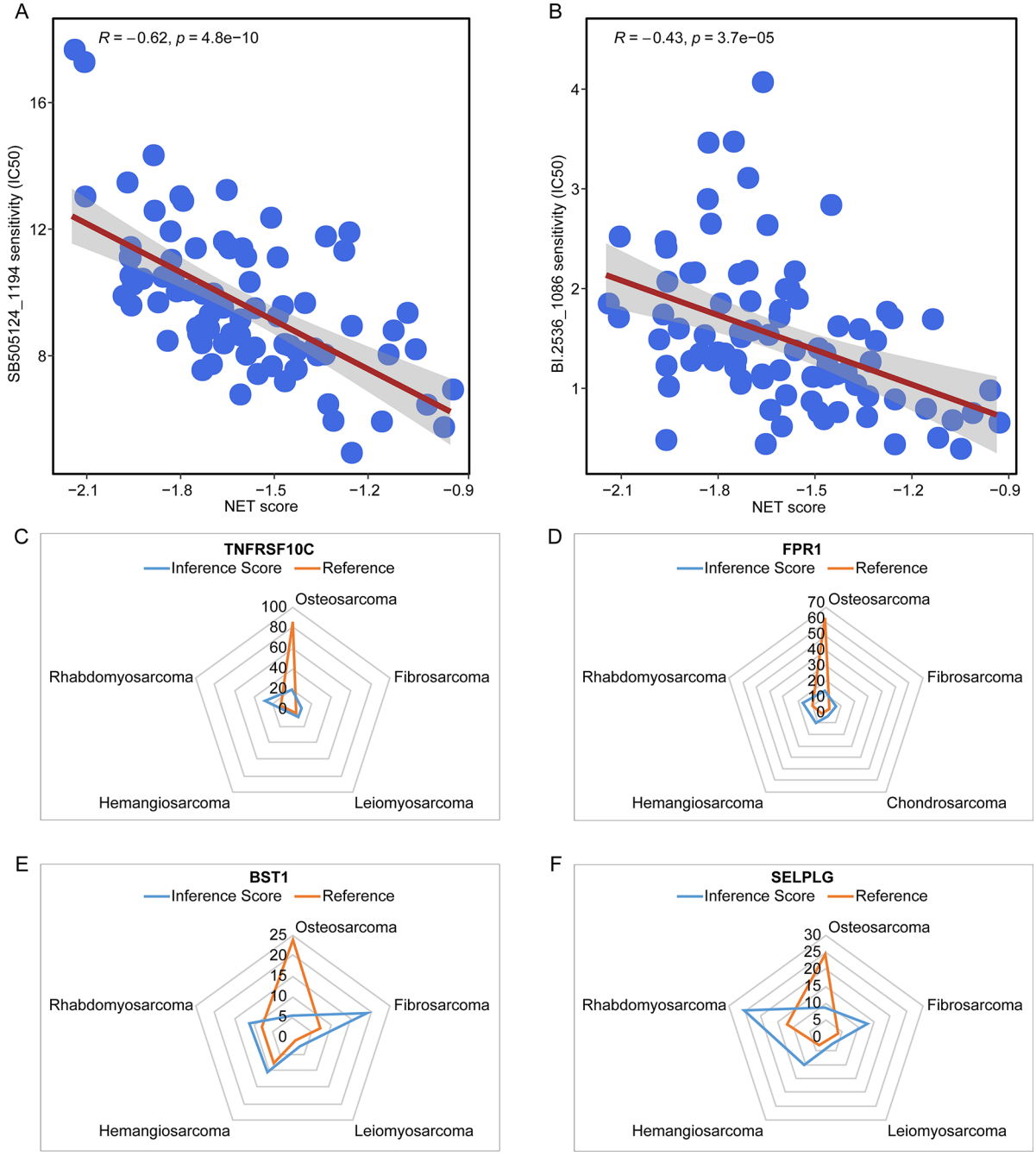

Fig. 4 Predictive value of NET score in anti-tumor agents. (**A**, **B**) The correlation between NET score and the IC50 value of SB505124_1194 and BI.2536_1086, respectively. Horizontal axis indicates NET score; vertical axis represents the IC50 value of drug (**C, D, E, F**) CTD database identified inference score of NET-related genes including TNERSF10C, FPR1, BST1 and SELPLG in OS

patients with high-NET scores had shortened survival outcomes. Moreover, within each subgroup, including age, gender or metastasis condition, OS patients with high-NET scores consistently exhibited reduced survival compared to those with low NET scores. These results collectively demonstrated that the NET signature model may offer robust predictive capability for OS prognosis.

Furthermore, scRNA-seq was then employed to verify the role of NET score in OS at a single cell resolution. Our data showed that OS cells progressively evolved into tumors characterized by a high NET score at the single cell resolution. Meanwhile, the intercellular communication between OS cells and other cells in the TME was analyzed based on the scRNA-seq data [55, 56]. In the high-NET group, checkpoint (CD24), cytokine

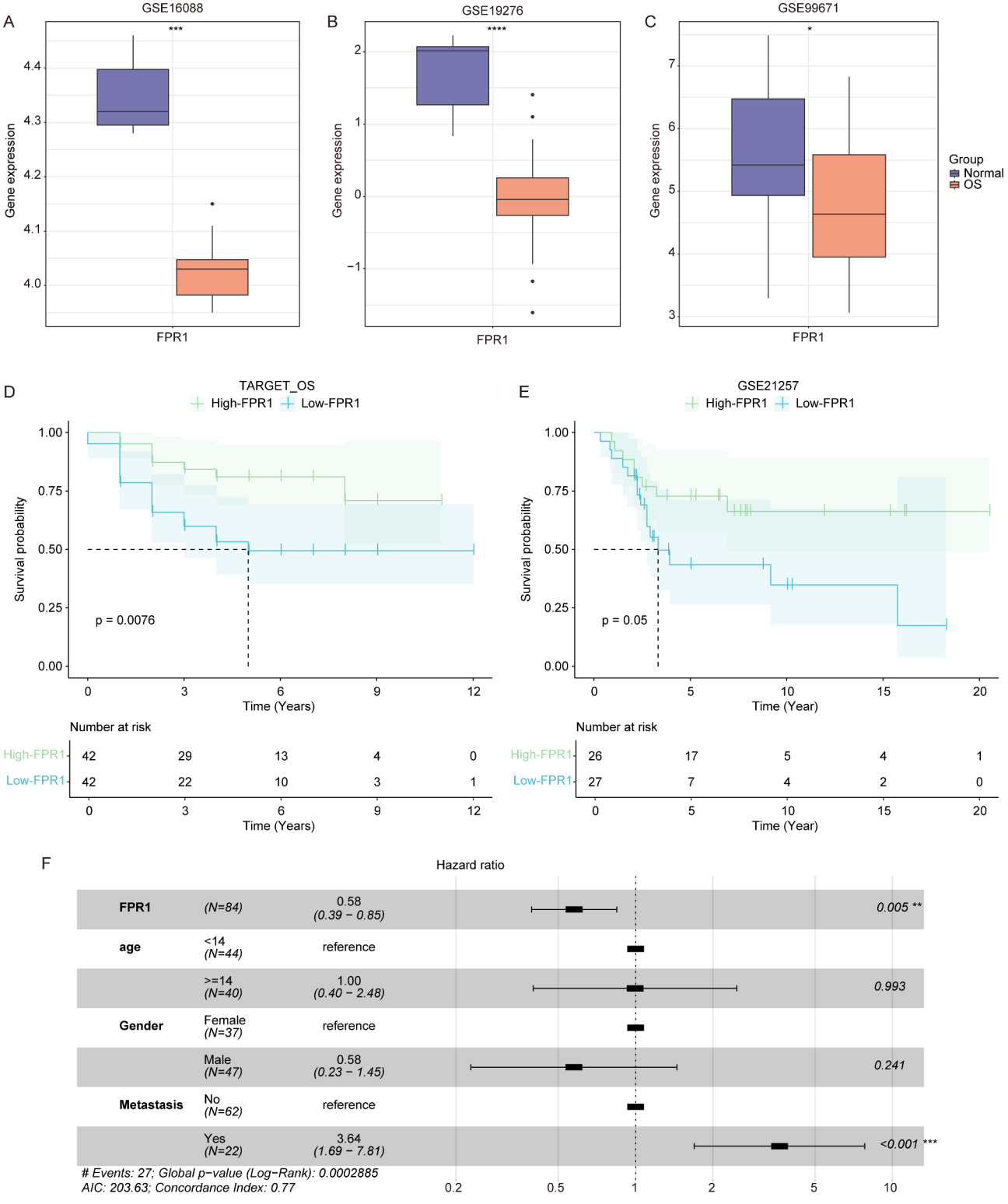

Fig. 5 Prognostic value of FPR1 score in OS (**A, B, C**) The box plot of FPR1 levels in normal and OS groups in the (**A**) GSE16088, (**B**) GSE19276 and (**C**) GSE99671 datasets (**D, E**) Kaplan-Meier survival curves of the overall survival for OS patients between the high-FPR1 and low-FPR1 groups in the (**D**) TARGET_OS cohort and (**E**) GSE21257 cohort (**F**) The multivariate Cox regression analyses about FPR1 gene and clinical factors in the TARGET_OS cohort

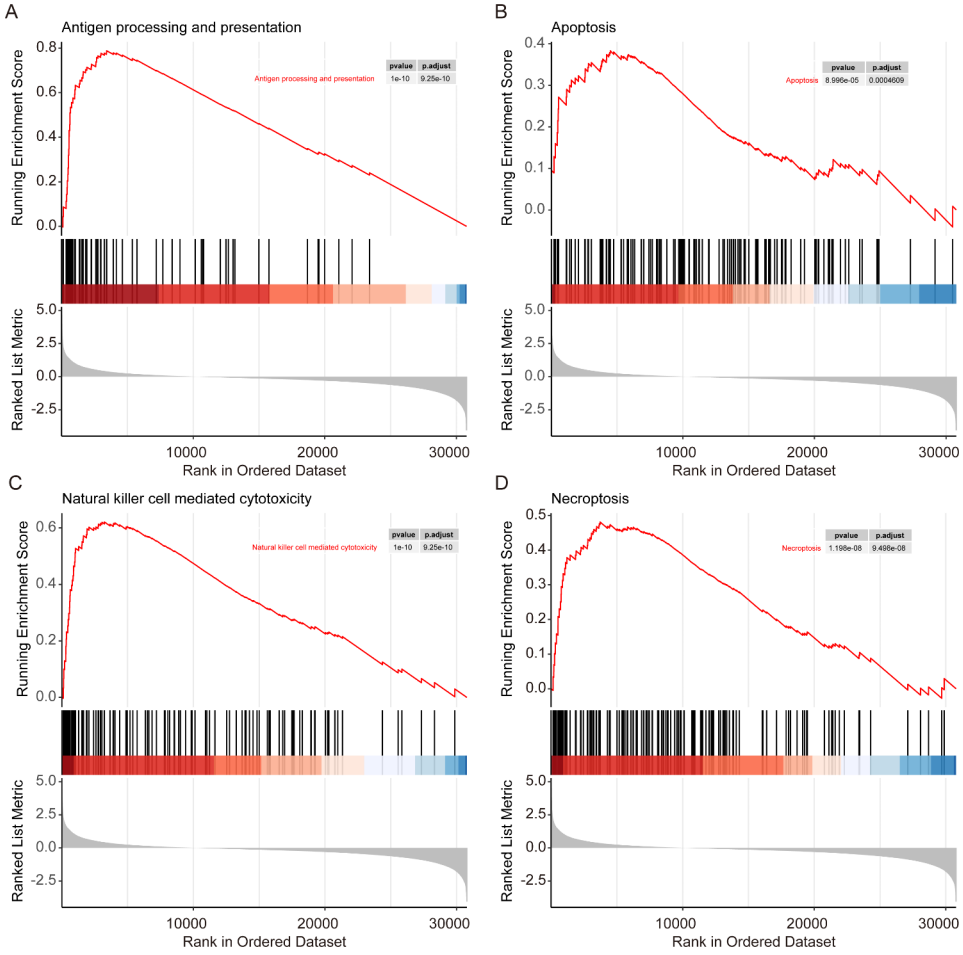

Fig. 6 The GSEA analysis based on FPR1 (**A, B, C, D**) Four signaling pathways enriched in high-FPR1 group identified by GSEA, including (**A**) Antigen processing and presentation, (**B**) Apoptosis, (**C**) Natural killer cell mediated cytotoxicity and (**D**) Necroptosis

(CXCL12), and other (TIMP1) were the most active CSPs participated in the intercellular communication between OS and other cells in the TME. CD24 and CXCL12, both recognized as oncogenes, have been shown to tumor progression and metastasis [57, 58]. Moreover, CD24 has been reported to accelerate the progression of hepatocellular carcinoma via modulating the TME [59]. Likewise, TIMP1, also classified as an oncogene, has been implicated in facilitating tumor progression and contributing to NET formation in tumors [22, 60, 61]. These data showed that cell communication between OS cells and other cells in the TME may exert a crucial role in tumor progression among OS patients with a high NET score.

Furthermore, we found that the NET score was notably negatively correlated with two drugs, SB505124_1194 (a selective TGFβR inhibitor) and BI.2536_1086 (PLK inhibitor), suggesting that patients with high-NET scores may be more sensitive to these two drugs. It has been shown that BI.2536 is currently in the phase I/II clinical research stage for various cancers [62, 63]. However, it has not yet progressed the clinical research in OS. Evidence has shown that inhibition of PLK could inhibit the progression of OS [64]. Thus, the findings may offer a valuable research direction for future clinical investigations involving BI.2536.

Additionally, CTD database revealed that these four NET-associated genes may serve as the potential therapeutic targets for OS. Meanwhile, TNFRSF10C and FPR1 appear to exert a strong value in the development and occurrence of OS. The involvement of TNFRSF10C in OS progression has been studied [50]. Consequently, we aimed to investigate the prognostic significance and biological function of FPR1 in OS. FPR1, a pattern-recognition receptor, has the potential to innate immune responses [65]. Notably, FPR1 can act as a tumor suppressor gene or oncogene in different cancer types [27, 28, 66]. Snapkov et al. found that overexpression of FPR1 can promote neuroblastoma tumorigenesis, with its elevated expression correlated to poor patient survival in neuroblastoma [66]. Conversely, Prevete et al. reported that FPR1 overexpression can suppress the tumorigenesis and angiogenesis in gastric cancer [28]. Consistently, our

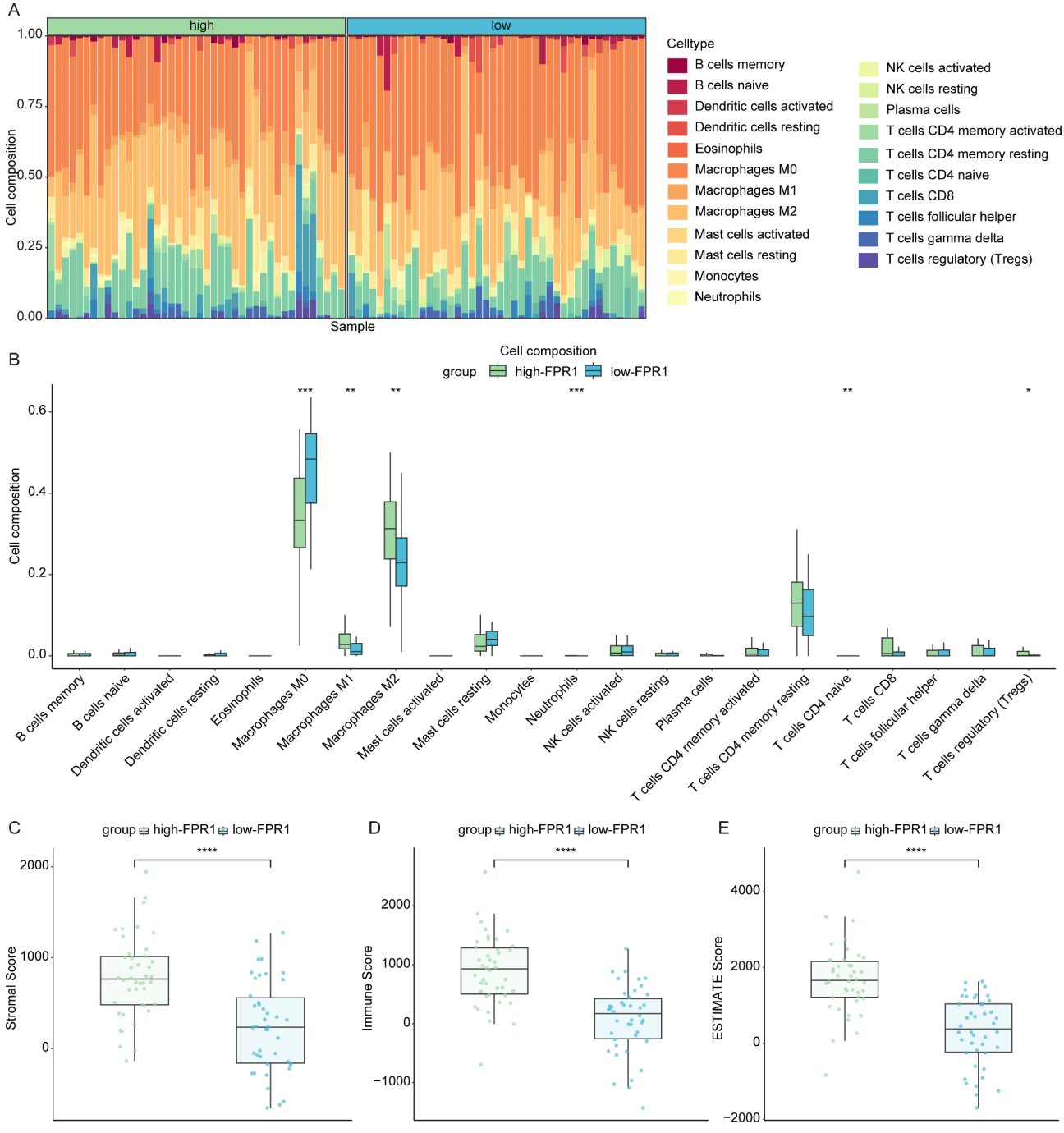

Fig. 7 Predictive value of NET score in immune microenvironment of OS (**A**) Bar plot displayed the proportions of the 22 types of infiltrated immune cells by the CIBERSORT algorithm in the TARGET_OS cohort (**B**) The box plots displayed the proportions of 22 immune cells in high-FPR1 and low-FPR1 groups by the CIBERSORT algorithm in the TARGET_OS cohort (**C, D, E**) ESTIMATE method was performed to evaluate the stromal score, immune score and ESTIMATE score in the TARGET_OS cohort between OS patients with high-FPR1 and low-FPR1 scores

results showed that overexpression of FPR1 significantly suppressed OS cell viability, migration and invasion, suggesting that it plays a tumor-suppressive role in OS. These findings illustrated that FPR1 can act as either an oncogene or a tumor suppressor across different tumor models. Furthermore, we present the novel discovery that high FPR1 expression is associated with better prognosis in OS patients. Our results suggest that FPR1 may function as a tumor-suppressor and may be a novel potential prognostic factor of OS.

Next, to explore the mechanisms underlying the FPR1 in OS, GSEA was performed. The results showed that

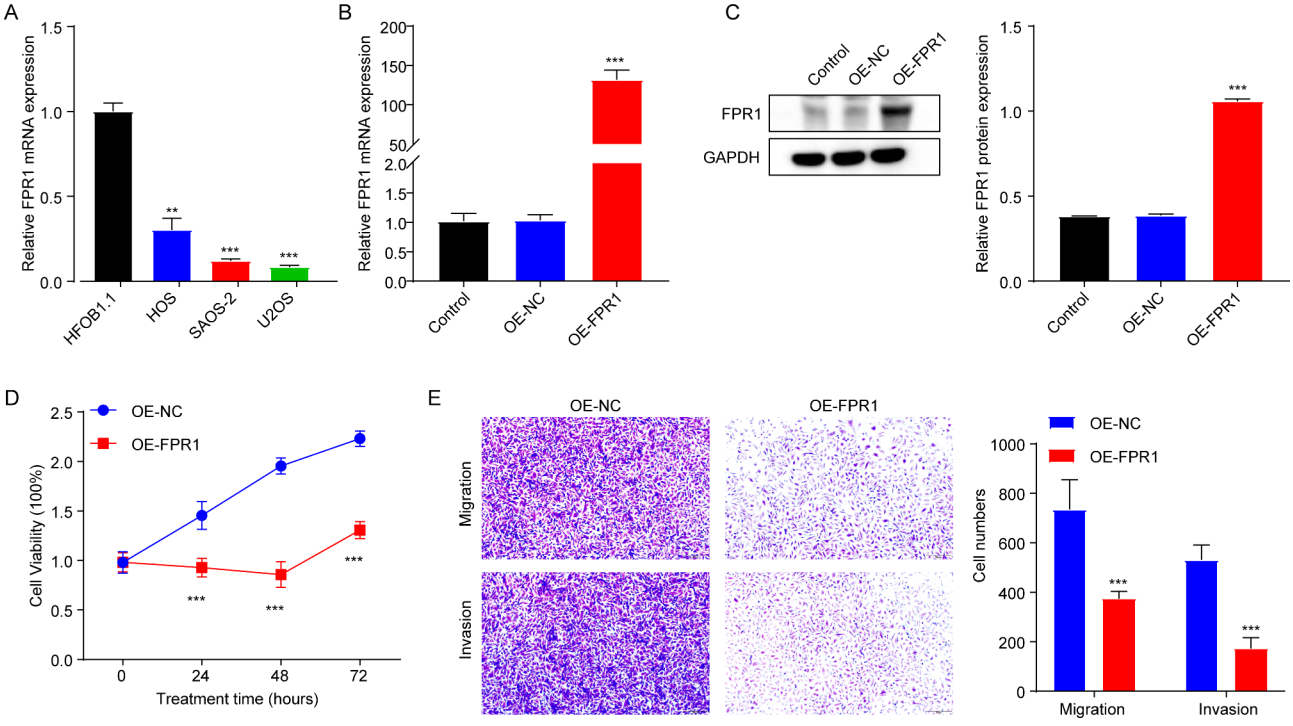

Fig. 8 Overexpression of FPR1 suppressed the viability, migration and invasion of OS cells (**A**) RT-qPCR analysis of FPR1 levels in HFOB1.19, HOS, SAOS-2 and U2OS cells (one-way ANOVA, compared to HFOB1.19 cells, $^{**}p < 0.01$, $^{***}p < 0.001$) (**B**) RT-qPCR and (**C**) western blot analysis of FPR1 levels in U2OS cells transfected with OE-NC and OE-FPR1 (one-way ANOVA, compared to OE-NC group, $^{***}p < 0.001$) (**D, E**) U2OS cells were transfected with OE-NC and OE-FPR1. (**D**) CCK-8 assay was used to evaluate cell viability; (**E**) Transwell assay was performed to assess cell migration and invasion (two-way ANOVA, compared to OE-NC group, $^{***}p < 0.001$)

necroptosis and apoptosis signaling pathways were significantly enriched in the high-FPR1 group. Our results showed that FPR could inhibit the progression of OS in vitro. However, whether FPR1 exerts an anti-tumor effect in OS through modulating cell apoptosis and necroptosis remains largely unclear and warrants further investigation. Additionally, some anti-tumor immune signaling pathways, including antigen processing and presentation and natural killer cell mediated cytotoxicity signalings, were also enriched in the high-FPR1 group. Evidence has demonstrated that TIME plays important roles in OS development [67], which is related to the tumorigenesis, metastasis and occurrence of tumors [10, 68]. It has been shown that M1 macrophages, as classical antigen-presenting cells, effectively capture and process antigens, thereby activating anti-tumor T cell responses [69]. Conversely, cancer patients with higher levels of M0 macrophages infiltration suffered from poorer prognosis [70]. In this study, we observed a significant increase in M1 macrophage infiltration in the high-FPR1 group, and patients with high-FPR1 was associated with good prognosis; whereas in the low-FPR1 group, there was a significant increase in M0 macrophage infiltration, which was associated with a poorer prognosis. These findings suggest that the differing states of macrophages may be a potential factor contributing to the variation in prognosis among patients with differing FPR1 levels.

Conclusion

Collectively, our study demonstrates that the NET-related gene FPR1 can suppress the progression of OS in vitro. Furthermore, FPR1 is closely associated with the prognosis and immune infiltration in OS. These results suggest that FPR1 may serve as a promising prognostic and therapeutic target in OS. However, the mechanisms underlying the role of FPR1 in OS has not yet been fully elucidated and require further investigation.

Abbreviations

OS	Osteosarcoma
TME	Tumor microenvironment
TIME	Tumor immune microenvironment
NET	Neutrophil extracellular traps
ROC	Receiver operating characteristic
AUC	Under the curves
DEGs	Differentially expressed genes
ScRNA-seq	Single-cell RNA-sequencing
TNFRSF10C	Tumor necrosis factor receptor superfamily, member 10c
FPR1	Formyl peptide receptor 1
BST1	Bone marrow stromal cell antigen-1
SELPLG	Selectin P ligand gene
Expr	Expression values
CTD	Comparative Toxicogenomics Database
GSVA	Gene Set Variation Analysis
GO	Gene Ontology

KEGG	Kyoto Encyclopedia of Genes and Genomes
GSVA	Gene Set Variation Analysis

Supplementary Information

The online version contains supplementary material available at https://doi.org/10.1186/s12891-024-08231-1.

Supplementary Material 1: Figure S1

Supplementary Material 2: Figure S2

Supplementary Material 3: Figure S3

Supplementary Material 4

Supplementary Material 5: Table S1

Supplementary Material 6: Table S2

Supplementary Material 7: Table S3

Supplementary Material 8: Table S4

Supplementary Material 9: Table S5

Supplementary Material 10: Table S6

Supplementary Material 11: Table S7

Supplementary Material 12: Table S8

Acknowledgements
Not applicable.

Author contributions
SHL and QY conceived the study; SHL and QY guided the methods; SHL and HYZ performed the software; SHL and QY analyzed the data; QY and HYZ collected the data; SHL and QY drafted the original manuscript; SHL and HYZ reviewed and edited the article; QY and HYZ visualized the study; SHL and HYZ administrated the project; YYZ made a lot of contribution during revision. All authors read and approved the final version to be published.

Funding
Not applicable.

Data availability
The data that support the findings of this study are available in the TARGET database (https://ocg.cancer.gov/programs/target), Gene Expression Omnibus (GEO) database (https://www.ncbi.nlm.nih.gov/geo/), Molecular Signature Database (https://www.gsea-msigdb.org/gsea/msigdb), CellMarker database (http://bio-bigdata.hrbmu.edu.cn/CellMarker/), Comparative Toxicogenomics Database (CTD) database (http://ctdbase.org/).

Declarations

Ethics approval and consent to participate
Not applicable.

Consent for publication
Not applicable.

Competing interests
The authors declare no competing interests.

Author details
[1]Department of Orthopedics, Zibo Central Hospital, West Campus, Zhangdian District, Zibo, Shandong Province 255036, P.R. China
[2]Department of Anesthesiology and Surgery, Zibo Central Hospital, Zhangdian District, Zibo, Shandong Province 255036, P.R. China
[3]Department of Hand & Foot Surgery, Zibo Central Hospital, Zibo, Shandong Province 255036, P.R. China
[4]Department of Hand & Foot Surgery, Zibo Central Hospital, No.54 Gongqingtuan West Road, Zhangdian District, Zibo, Shandong Province 255036, P.R. China

Received: 15 September 2023 / Accepted: 20 December 2024
Published online: 31 March 2025

References

1. Song XJ, Bi MC, Zhu QS, Liu XL. The emerging role of lncRNAs in the regulation of osteosarcoma stem cells. Eur Rev Med Pharmacol Sci. 2022;26(3):966–74.
2. Cersosimo F, Lonardi S, Bernardini G, Telfer B, Mandelli GE, Santucci A et al. Tumor-Associated macrophages in Osteosarcoma: from mechanisms to Therapy. Int J Mol Sci. 2020;21(15):5207.
3. Chen C, Xie L, Ren T, Huang Y, Xu J, Guo W. Immunotherapy for osteosarcoma: fundamental mechanism, rationale, and recent breakthroughs. Cancer Lett. 2021;500:1–10.
4. Garcia-Ortega DY, Cabrera-Nieto SA, Caro-Sanchez HS, Cruz-Ramos M. An overview of resistance to chemotherapy in osteosarcoma and future perspectives. Cancer Drug Resist. 2022;5(3):762–93.
5. Hu Z, Wen S, Huo Z, Wang Q, Zhao J, Wang Z, et al. Current status and prospects of targeted therapy for Osteosarcoma. Cells. 2022;11:21.
6. Wang G, Zhang X, Feng W, Wang J. Prediction of prognosis and immunotherapy of Osteosarcoma based on necroptosis-related lncRNAs. Front Genet. 2022;13:917935.
7. Marshall SK, Saelim B, Taweesap M, Pachana V, Panrak Y, Makchuchit N et al. Anti-EGFR targeted multifunctional I-131 radio-nanotherapeutic for treating Osteosarcoma: in Vitro 3D Tumor Spheroid Model. Nanomaterials (Basel). 2022;12(19):3517.
8. Yang M, Zheng H, Xu K, Yuan Q, Aihaiti Y, Cai Y, et al. A novel signature to guide osteosarcoma prognosis and immune microenvironment: cuproptosis-related lncRNA. Front Immunol. 2022;13:919231.
9. Xia Y, Wang D, Piao Y, Chen M, Wang D, Jiang Z, et al. Modulation of immunosuppressive cells and noncoding RNAs as immunotherapy in osteosarcoma. Front Immunol. 2022;13:1025532.
10. Liu W, Hu H, Shao Z, Lv X, Zhang Z, Deng X, et al. Characterizing the tumor microenvironment at the single-cell level reveals a novel immune evasion mechanism in osteosarcoma. Bone Res. 2023;11(1):4.
11. Chiang CC, Cheng WJ, Korinek M, Lin CY, Hwang TL. Neutrophils in Psoriasis. Front Immunol. 2019;10:2376.
12. Zheng Z, Xu Y, Shi Y, Shao C. Neutrophils in the tumor microenvironment and their functional modulation by mesenchymal stromal cells. Cell Immunol. 2022;379:104576.
13. Mizuno R, Kawada K, Itatani Y, Ogawa R, Kiyasu Y, Sakai Y. The role of Tumor-Associated neutrophils in Colorectal Cancer. Int J Mol Sci. 2019;20(3):529.
14. Jaillon S, Ponzetta A, Di Mitri D, Santoni A, Bonecchi R, Mantovani A. Neutrophil diversity and plasticity in tumour progression and therapy. Nat Rev Cancer. 2020;20(9):485–503.
15. Lu J, Peng Y, Huang R, Feng Z, Fan Y, Wang H, et al. Elevated TYROBP expression predicts poor prognosis and high tumor immune infiltration in patients with low-grade glioma. BMC Cancer. 2021;21(1):723.
16. Yazdani HO, Roy E, Comerci AJ, van der Windt DJ, Zhang H, Huang H, et al. Neutrophil Extracellular traps Drive mitochondrial homeostasis in tumors to augment growth. Cancer Res. 2019;79(21):5626–39.
17. Lee KH, Kronbichler A, Park DD, Park Y, Moon H, Kim H, et al. Neutrophil extracellular traps (NETs) in autoimmune diseases: a comprehensive review. Autoimmun Rev. 2017;16(11):1160–73.
18. Zhou J, Yang Y, Gan T, Li Y, Hu F, Hao N, et al. Lung cancer cells release high mobility group box 1 and promote the formation of neutrophil extracellular traps. Oncol Lett. 2019;18(1):181–8.
19. Zhang L, Yi H, Chen J, Li H, Luo Y, Cheng T, et al. Neutrophil Extracellular traps Facilitate A549 Cell Invasion and Migration in a macrophage-maintained inflammatory microenvironment. Biomed Res Int. 2022;2022:8316525.
20. Yang L, Liu Q, Zhang X, Liu X, Zhou B, Chen J, et al. DNA of neutrophil extracellular traps promotes cancer metastasis via CCDC25. Nature. 2020;583(7814):133–8.
21. Zha C, Meng X, Li L, Mi S, Qian D, Li Z, et al. Neutrophil extracellular traps mediate the crosstalk between glioma progression and the tumor microenvironment via the HMGB1/RAGE/IL-8 axis. Cancer Biology Med. 2020;17(1):154–68.

22. Schoeps B, Eckfeld C, Prokopchuk O, Bottcher J, Haussler D, Steiger K, et al. TIMP1 triggers Neutrophil Extracellular trap formation in pancreatic Cancer. Cancer Res. 2021;81(13):3568–79.
23. Jiang T, Wang Y, Chen X, Xia W, Xue S, Gu L, et al. Neutrophil extracellular traps (NETs)-related lncRNAs signature for predicting prognosis and the immune microenvironment in breast cancer. Front Cell Dev Biol. 2023;11:1117637.
24. Quan J, Huang B. Identification and validation of the molecular subtype and prognostic signature for clear cell renal cell carcinoma based on neutrophil extracellular traps. Front Cell Dev Biol. 2022;10:1021690.
25. Ding W, Li B, Zhang Y, He L, Su J. A neutrophil extracellular traps-associated lncRNA signature predicts the clinical outcomes in patients with lung adenocarcinoma. Front Genet. 2022;13:1047231.
26. Li Q, Chen W, Li Q, Mao J, Chen X. A novel neutrophil extracellular trap signature to predict prognosis and immunotherapy response in head and neck squamous cell carcinoma. Front Immunol. 2022;13:1019967.
27. Le Naour J, Montegut L, Pan Y, Scuderi SA, Cordier P, Joseph A, et al. Formyl peptide receptor-1 (FPR1) represses intestinal oncogenesis. Oncoimmunology. 2023;12(1):2237354.
28. Prevete N, Liotti F, Illiano A, Amoresano A, Pucci P, de Paulis A, et al. Formyl peptide receptor 1 suppresses gastric cancer angiogenesis and growth by exploiting inflammation resolution pathways. Oncoimmunology. 2017;6(4):e1293213.
29. Xie L, Zeng J, He M. Identification and verification of a BMPs-related gene signature for osteosarcoma prognosis prediction. BMC Cancer. 2023;23(1):181.
30. Liu Y, Feng W, Dai Y, Bao M, Yuan Z, He M, et al. Single-cell Transcriptomics reveals the complexity of the Tumor Microenvironment of Treatment-Naive Osteosarcoma. Front Oncol. 2021;11:709210.
31. Rothzerg E, Feng W, Song D, Li H, Wei Q, Fox A, et al. Single-cell transcriptome analysis reveals paraspeckles expression in Osteosarcoma tissues. Cancer Inf. 2022;21:11769351221140101.
32. Friedman J, Hastie T, Tibshirani R. Regularization paths for generalized Linear models via Coordinate Descent. J Stat Softw. 2010;33(1):1–22.
33. Lei T, Qian H, Lei P, Hu Y. Ferroptosis-related gene signature associates with immunity and predicts prognosis accurately in patients with osteosarcoma. Cancer Sci. 2021;112(11):4785–98.
34. Wang L, Qiu M, Wu L, Li Z, Meng X, He L, et al. Construction and validation of prognostic signature for hepatocellular carcinoma basing on hepatitis B virus related specific genes. Infect Agents cancer. 2022;17(1):60.
35. Blanche P, Dartigues JF, Jacqmin-Gadda H. Estimating and comparing time-dependent areas under receiver operating characteristic curves for censored event times with competing risks. Stat Med. 2013;32(30):5381–97.
36. Chen Y, Lun AT, Smyth GK. From reads to genes to pathways: differential expression analysis of RNA-Seq experiments using rsubread and the edgeR quasi-likelihood pipeline. F1000Res. 2016;5:1438.
37. Yu G, Wang LG, Han Y, He QY. clusterProfiler: an R package for comparing biological themes among gene clusters. OMICS. 2012;16(5):284–7.
38. Hao Y, Hao S, Andersen-Nissen E, Mauck WM 3rd, Zheng S, Butler A, et al. Integrated analysis of multimodal single-cell data. Cell. 2021;184(13):3573–e8729.
39. Zhang L, Wu S, Huang J, Shi Y, Yin Y, Cao X. A mitochondria-related signature for predicting immune microenvironment and therapeutic response in osteosarcoma. Front Oncol. 2022;12:1085065.
40. Qiu X, Hill A, Packer J, Lin D, Ma YA, Trapnell C. Single-cell mRNA quantification and differential analysis with Census. Nat Methods. 2017;14(3):309–15.
41. Love MI, Huber W, Anders S. Moderated estimation of Fold change and dispersion for RNA-seq data with DESeq2. Genome Biol. 2014;15(12):550.
42. Newman AM, Liu CL, Green MR, Gentles AJ, Feng W, Xu Y, et al. Robust enumeration of cell subsets from tissue expression profiles. Nat Methods. 2015;12(5):453–7.
43. Gao Y, Liu L, Zhang Z, Qin C, Yang B, Ke Y. TYRP1 protects against the apoptosis and oxidative stress of retinal ganglion cells by binding to PMEL. Ocul Immunol Inflamm. 2023;31(5):1024–34.
44. Yaykasli KO, Schauer C, Munoz LE, Mahajan A, Knopf J, Schett G et al. Neutrophil Extracell Trap-Driven Occlusive Diseases. Cells. 2021;10(9):2208.
45. Wang Y, Liu F, Chen L, Fang C, Li S, Yuan S, et al. Neutrophil Extracellular traps (NETs) promote Non-small Cell Lung Cancer Metastasis by suppressing lncRNA MIR503HG to activate the NF-kappaB/NLRP3 inflammasome pathway. Front Immunol. 2022;13:867516.
46. Chen Y, Hu H, Tan S, Dong Q, Fan X, Wang Y, et al. The role of neutrophil extracellular traps in cancer progression, metastasis and therapy. Exp Hematol Oncol. 2022;11(1):99.
47. Yang J, Jin L, Kim HS, Tian F, Yi Z, Bedi K, et al. KDM6A loss recruits Tumor-Associated neutrophils and promotes Neutrophil Extracellular trap formation in pancreatic Cancer. Cancer Res. 2022;82(22):4247–60.
48. Tu Y, Mao Z. Identification and validation of Molecular Subtype and Prognostic signature for bladder Cancer based on Neutrophil Extracellular traps. Cancer Invest. 2023;41(4):354–68.
49. Song D, Yin X, Che C. Distinct Gene Expression and Immune Features Between Different Neutrophil Extracellular Trap-Related Osteosarcoma Subtypes. Applied biochemistry and biotechnology. 2025;197(1):55-72.
50. Feng W, Lin H, Rothzerg E, Song D, Zhao W, Ning T, et al. RNA-seq and single-cell transcriptome analyses of TRAIL receptors Gene expression in human osteosarcoma cells and tissues. Cancer Inform. 2023;22:11769351231161478.
51. Lopatina O, Yoshihara T, Nishimura T, Zhong J, Akther S, Fakhrul AA, et al. Anxiety- and depression-like behavior in mice lacking the CD157/BST1 gene, a risk factor for Parkinson's disease. Front Behav Neurosci. 2014;8:133.
52. Ortolan E, Giacomino A, Martinetto F, Morone S, Lo Buono N, Ferrero E, et al. CD157 enhances malignant pleural mesothelioma aggressiveness and predicts poor clinical outcome. Oncotarget. 2014;5(15):6191–205.
53. Wang B, Sun Y. SELPLG expression was potentially correlated with metastasis and prognosis of Osteosarcoma. Pathol Oncol Res. 2022;28:1610047.
54. Cheng TY, Wu MS, Lin JT, Lin MT, Shun CT, Hua KT, et al. Formyl peptide receptor 1 expression is associated with tumor progression and survival in gastric cancer. Anticancer Res. 2014;34(5):2223–9.
55. Jin S, Guerrero-Juarez CF, Zhang L, Chang I, Ramos R, Kuan CH, et al. Inference and analysis of cell-cell communication using CellChat. Nat Commun. 2021;12(1):1088.
56. Kalluri R, McAndrews KM. The role of extracellular vesicles in cancer. Cell. 2023;186(8):1610–26.
57. Lee JH, Kim SH, Lee ES, Kim YS. CD24 overexpression in cancer development and progression: a meta-analysis. Oncol Rep. 2009;22(5):1149–56.
58. Ma JC, Sun XW, Su H, Chen Q, Guo TK, Li Y, et al. Fibroblast-derived CXCL12/SDF-1alpha promotes CXCL6 secretion and co-operatively enhances metastatic potential through the PI3K/Akt/mTOR pathway in colon cancer. World J Gastroenterol. 2017;23(28):5167–78.
59. Wan X, Cheng C, Shao Q, Lin Z, Lu S, Chen Y. CD24 promotes HCC progression via triggering notch-related EMT and modulation of tumor microenvironment. Tumour Biol. 2016;37(5):6073–84.
60. Song G, Xu S, Zhang H, Wang Y, Xiao C, Jiang T, et al. TIMP1 is a prognostic marker for the progression and metastasis of colon cancer through FAK-PI3K/AKT and MAPK pathway. J Exp Clin Cancer Res. 2016;35(1):148.
61. Liu H, Xiang Y, Zong QB, Zhang XY, Wang ZW, Fang SQ, et al. Mir-6745-TIMP1 axis inhibits cell growth and metastasis in gastric cancer. Aging. 2021;13(21):24402–16.
62. Awad MM, Chu QS, Gandhi L, Stephenson JJ, Govindan R, Bradford DS, et al. An open-label, phase II study of the polo-like kinase-1 (Plk-1) inhibitor, BI 2536, in patients with relapsed small cell lung cancer (SCLC). Lung Cancer. 2017;104:126–30.
63. Muller-Tidow C, Bug G, Lubbert M, Kramer A, Krauter J, Valent P, et al. A randomized, open-label, phase I/II trial to investigate the maximum tolerated dose of the Polo-like kinase inhibitor BI 2536 in elderly patients with refractory/relapsed acute myeloid leukaemia. Br J Haematol. 2013;163(2):214–22.
64. Cheng L, Wang C, Jing J. Polo-like kinase 1 as a potential therapeutic target for osteosarcoma. Curr Pharm Design. 2015;21(10):1347–50.
65. Petrazzuolo A, Le Naour J, Vacchelli E, Gaussem P, Ellouze S, Jourdi G, et al. No impact of cancer and plague-relevant FPR1 polymorphisms on COVID-19. Oncoimmunology. 2020;9(1):1857112.
66. Snapkov I, Oqvist CO, Figenschau Y, Kogner P, Johnsen JI, Sveinbjornsson B. The role of formyl peptide receptor 1 (FPR1) in neuroblastoma tumorigenesis. BMC Cancer. 2016;16:490.
67. Zhang W, Lyu P, Andreev D, Jia Y, Zhang F, Bozec A. Hypoxia-immune-related microenvironment prognostic signature for osteosarcoma. Front Cell Dev Biol. 2022;10:974851.
68. Luo ZW, Liu PP, Wang ZX, Chen CY, Xie H. Macrophages in Osteosarcoma Immune Microenvironment: implications for Immunotherapy. Front Oncol. 2020;10:586580.
69. Ahmad A. Epigenetic regulation of immunosuppressive tumor-associated macrophages through dysregulated microRNAs. Semin Cell Dev Biol. 2022;124:26–33.

70. Xu X, Wang J. Prognostic prediction and multidimensional dissections of a macrophages M0-related gene signature in liver cancer. Front Endocrinol. 2023;14:1153562.

Publisher's note